Magnetocaloric effect of FeNi magnetic nanoparticles obtained by the electrical explosion of wire technique

© *G.V. Kurlyandskaya* [1], *A.V. Arkhipov* [1], *I.V. Beketov* [1,2], *A.V. Bagazeev* [2], *A.S. Volegov* [1],
A. Larrañanga [3], *E.A. Mikhnevich* [1], *A.V. Svalov* [1]

[1] Institute of Natural Sciences and Mathematics,
Ural Federal University named after the First President of Russia B.N. Yeltsin,
Yekaterinburg, Russia
[3] The Basque Country University UPV-EHU,
Bilbao, Spain

E-mail: galinakurlyandskaya@urfu.ru

In this work the structure, magnetic properties and of the magnetocaloric effect of the large batches of magnetic FeNi nanoparticles were studied for selected compositions close to the invar. Nanoparticles were synthesized by the method of the electric explosion of wire using various technological parameters ensuring the difference in their dispersion parameters. The main variable parameter was the degree of overheating of the wire material. The use of different technological conditions for obtaining batches of nanoparticles ensured the difference in their dispersion parameters.

Keywords: electric explosion of wire, magnetic nanoparticles, invar composition, magnetic properties, magnetocaloric effect.

1. Introduction

Magnetic cooling technology is now regarded as a promising, efficient counterpart to modern compression cooling. It is based on the magnetocaloric effect (MCE) — the ability of magnetic materials to change their temperature under the influence of an external magnetic field [1]. The maximum value of the MCE is achieved near the phase transitions observed in the working magnetic material. The highest MCE is observed in materials which characterized by a phase transition of the first kind, with a relatively narrow temperature range; these materials are also characterized by hysteresis phenomena. For materials in which a magnetic phase transition of the second order is observed, the magnetocaloric peak is smaller, but the width of the temperature interval at which this peak is observed is much greater than in materials with a magnetic phase transition of the first order [2]. This increases the so-called relative cooling power (RCP) or cooling capacity, the value of which is defined as the product of the maximum magnitude of the peak change in the magnetic portion of the entropy ($\Delta S_{M(\max)}(T, H)$) and the width of this peak at half its height (δT_{FWHM}) [3].

Among the materials exhibiting magnetic phase transition of the second kind, gadolinium remains the most popular in terms of working material for the „magnetic cooler" due to its large MCE value and proximity of the Curie temperature to room temperature [3–5]. Transition metal alloys have a markedly lower MCE, but their advantages are high mechanical strength, corrosion resistance, negligible magnetic

hysteresis, easily varied Curie temperature, including in the temperature range above room values, which makes them a promising material for multistage magnetic cooling systems starting from temperatures above room temperature [2,6].

The task of improving the efficiency of heat transfer between the working body and the environment requires the use of magnetic materials for magnetic cooling devices in various forms, including in the form of powders and stabilized suspensions based on them [7–9].

The most common method of producing magnetocaloric powders is the ball mill method [7,9]. In recent years, the electrophysical method of electric explosion of the wire (EEW) has become widespread for obtaining very large batches of powders, making it possible to obtain both magnetic nanoparticles of pure materials (Co, Fe, Ni) and their alloys (FeNi, FeCo, etc.) and oxides, nitrides and carbides based on them [10,11]. The dispersion parameters of each batch of nanoparticles are related to the process parameters of EWE fusion, such as wire diameter, length of wire working section, capacitor battery charging voltage before each explosion, capacitor battery capacity, superheat factor (ratio of injected energy to sublimation energy of wire material), composition of gas mixture inside the blast chamber, etc. The gas system of the EWE unit contains separation devices to separate the produced nanoparticles into different size fractions [10,11]. Such a wide range of conditions for obtaining nanoparticles from the same material enables flexible adaptation of the functional properties of the powders by selecting the optimal

process parameters for obtaining and additional treatment of magnetic particles [11]. This opens up particular opportunities for optimizing the properties of magnetocaloric materials, whose nano-structuring not only makes it possible to vary the operating temperature ranges but also to modify the field dependence of the magnetocaloric effect [12,13]. In addition, in terms of applications, batch size often plays a key role. However, the development of nanomaterials in the laboratory often produces small batches, assuming that later adaptation of the technology in terms of larger batch sizes is necessary. The latter is not always possible. Therefore, research on large batch powders, rather than ideal powders, adapted to the task at hand can have a special role. Thus, in the case of MCE powders, it can be assumed that the width of the temperature interval in which the magnetocaloric peak is observed can vary due to variations in the dispersion parameters of the magnetic nanoparticle (MNP) lot. Thus, undesirable in the case of biomedical applications [14,15]. The batch size dispersion of EWE-MNP can be favorable under certain conditions when it comes to large batches of MNP for MCE applications.

This paper presents the results of studies of structural, magnetic and magnetocaloric properties of iron-nickel alloy nanoparticles of close to invar compositions produced by electrical wire explosion using different process conditions. In the analysis of large batches of nanoparticles, the evolution of ensemble dispersity features under successive changes of a significant parameter such as overheating during the explosion was considered.

2. Technique of studies

Four batches of EWE-MNP were produced using the same Fe — 64, Ni — 36% by weight, 0.25 mm diameter. The chamber of the EWE unit was filled with nitrogen at a pressure of 0.12 MPa at a circulation rate of 150 l/min, supported by a gas turbine. Due to the high pyrophoricity, the powders were passivated by adding a small amount of oxygen at $3 \cdot 10^{-2}$ l/min before extraction. Process parameters of obtaining by EWE method and some physical characteristics of batches of samples of FeNi magnetic nanoparticles are presented in Table 1, where K — over heating or ratio of energy input into wire (W_o), to sublimation energy of wire metal (W_s) for wire length l: $K = W_o/W_s$.

The energy injected into the wire depends on the capacitor bank (C) and the voltage of the charged capacitor bank (U_o) just before the explosion: $W_o = CU_o^2/2$.

In this problem formulation, a regular evolution of the dispersion parameters and the magnetocaloric effect can be traced as a function of the superheat level. Of particular note is the fact that the practice of working with nanoparticles very often seeks to obtain an ensemble of identical spherical particles by laboratory methods, but it is not always possible to transfer the conditions of the laboratory experiment to

Table 1. Synthesis conditions and some characteristics of batches of FeNi nanoparticles produced by the EWE method using different process parameters

Sample	l, cm	U_o, kV	C, μF	K	Composition	S_{sp}, m^2/g	d_w, nm
P1	7	30	3.2	2.3	Fe$_{61}$Ni$_{39}$	13.5	55
P2	7	30	1.6	1.9	Fe$_{62}$Ni$_{38}$	12.1	61
P3	7	20	1.6	1.2	Fe$_{63}$Ni$_{37}$	7.8	94
P4	10	20	1.6	0.8	Fe$_{64}$Ni$_{36}$	4.6	160

industrial technology. Here, large batches of nanoparticles with a wide size distribution are deliberately studied, and the technology to produce them does not require further adaptation. As will be shown, a broad size distribution can play a positive role under certain conditions. Moreover, the magnetocaloric effect can be considered as a tool in the validation of large batches of nanoparticles with a wide size distribution. In literature, there has not been much interest in such objects until recently. At the same time, the emergent interest in filled magnetic composites also requires the development of additional methods for attesting large batches of nanoparticles with a broad size distribution.

The sample composition was determined by fluorescence analysis (Fischerscope X-Ray system XDAL) and energy-dispersive X-ray spectroscopy (M3000 Hitachi, at 15 kV). The structure was analyzed by X-ray diffraction analysis (XRD, PANalytical Cubix3 at 40 kV and 40 mA) using CuK$_\alpha$-radiation and scanning electron microscopy (SEM) at an accelerating voltage of 20 kV. The specific surface area S_{sp} for each batch was determined using the standard Brunauer, Emmet and Teller (BET) method using low-temperature nitrogen sorption data (Micromeritics TriStar3000). The surface average particle diameter d_w was calculated using the known formula

$$d_w = \frac{6}{\rho S_{sp}}, \qquad (1)$$

where ρ — the density of the MNP material. The average particle diameter d_n was calculated as follows:

$$\frac{N}{N_0} = \frac{N(d)}{N_0} \cdot 100\%, \qquad (2)$$

where $N(d)$ — number of particles with diameter d; N_0 — particle number in the sample. The average particle diameter was calculated using ImageJ software. Based on the particle diameter values obtained, a Histogram was plotted in OriginPro, from which the mean diameter (d_n) and number (N) of the particles examined were determined. The resulting particle count data were substituted into formula 2.

Magnetic attestation (hysteresis loops and thermomagnetic curves) was carried out with a SQUID magnetometer. The temperature dependences of the change in the magnetic part of the entropy $\Delta S_M(T)$ were derived from Maxwell's
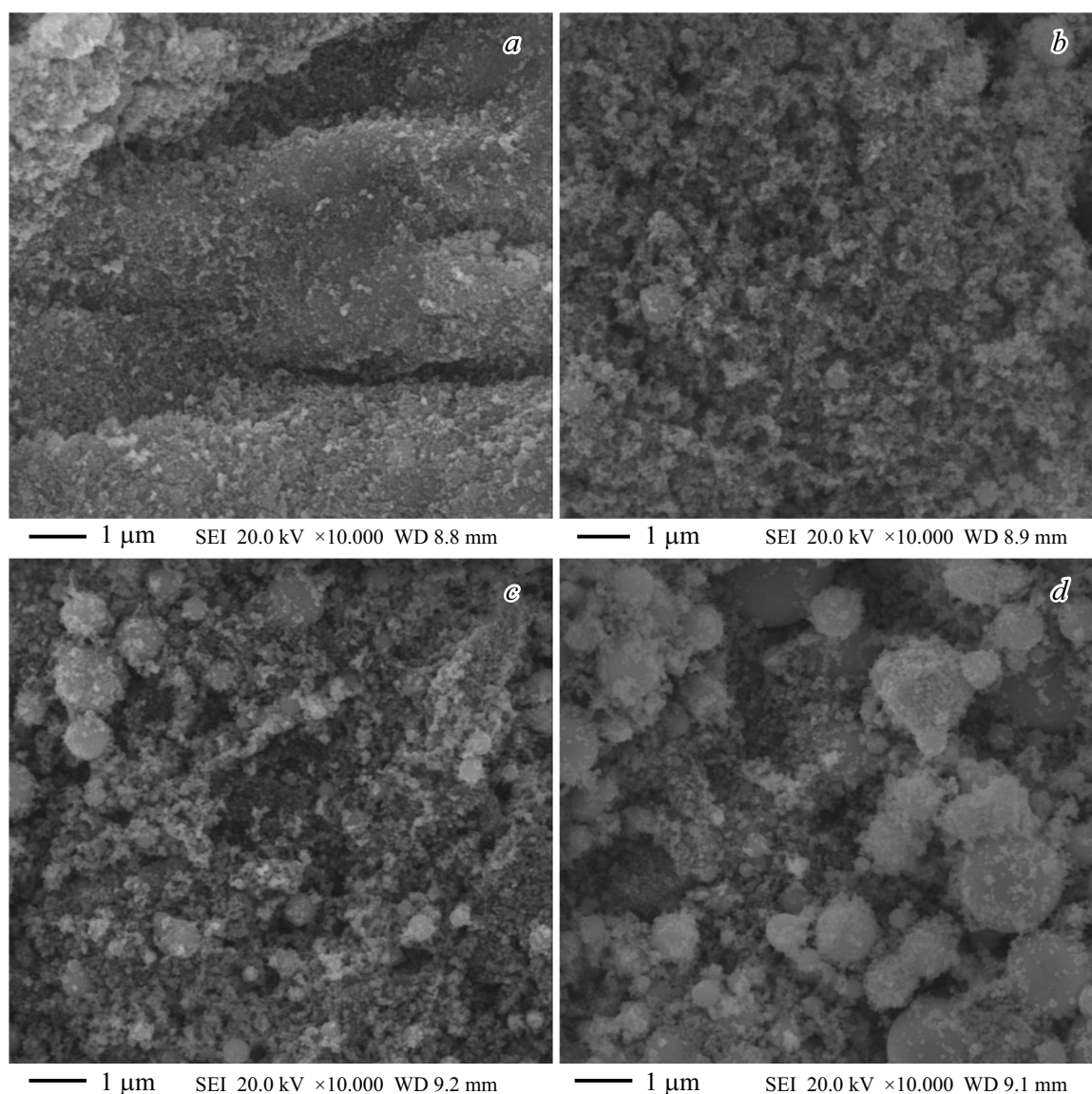
Figure 1. General view (SEM) of the MNP of the batches studied: a — P1; b — P2; c — P3; d — P4, at fairly low magnification.

relations using isothermal magnetization dependences in fields up to 7 T.

3. Results and discussion

Figure 1 shows SEM photographs at low magnification, allowing a qualitative assessment of the size distribution and shape of nanoparticles of different sizes. It can clearly be seen that the shape of the MNP of all lots and all sizes is close to spherical. According to the BET data, an increase in the superheat coefficient during MNP synthesis leads to an increase in their specific surface area (Figure 1, Table 1). In this case, it is to be expected that there are sufficient differences in the dispersion parameters of the different batches, the characteristics of which would be difficult to assess on the basis of their specific surface area data alone.

Thus, batch P1 is characterized by the presence of small MNP (less than 100 nm) with very few significantly larger particles (up to 1μm). Although the average visual size of the small MNP of batch P2 is only slightly higher than the average size of the small particles of batch P1, there are noticeably more MNP present in P2 whose size is close to 1.0μm. In batch P3 the number of MNP close to 1.0μm and above is already increasing markedly, and there is also an increase in the number of MNP „of medium size" around 0.5μm. Batch P4 is characterized by the presence of a significant number of very large particles $(1.0-2.0 \mu$m) and an increase in the number of medium-sized MNP, around 0.5μm, but visually it appears that very small MNP (less than 100 nm) are maintained or even increased in the P4 batch.

In order to quantitatively compare the dispersion features of the resulting lots of MNP, typical ensembles were
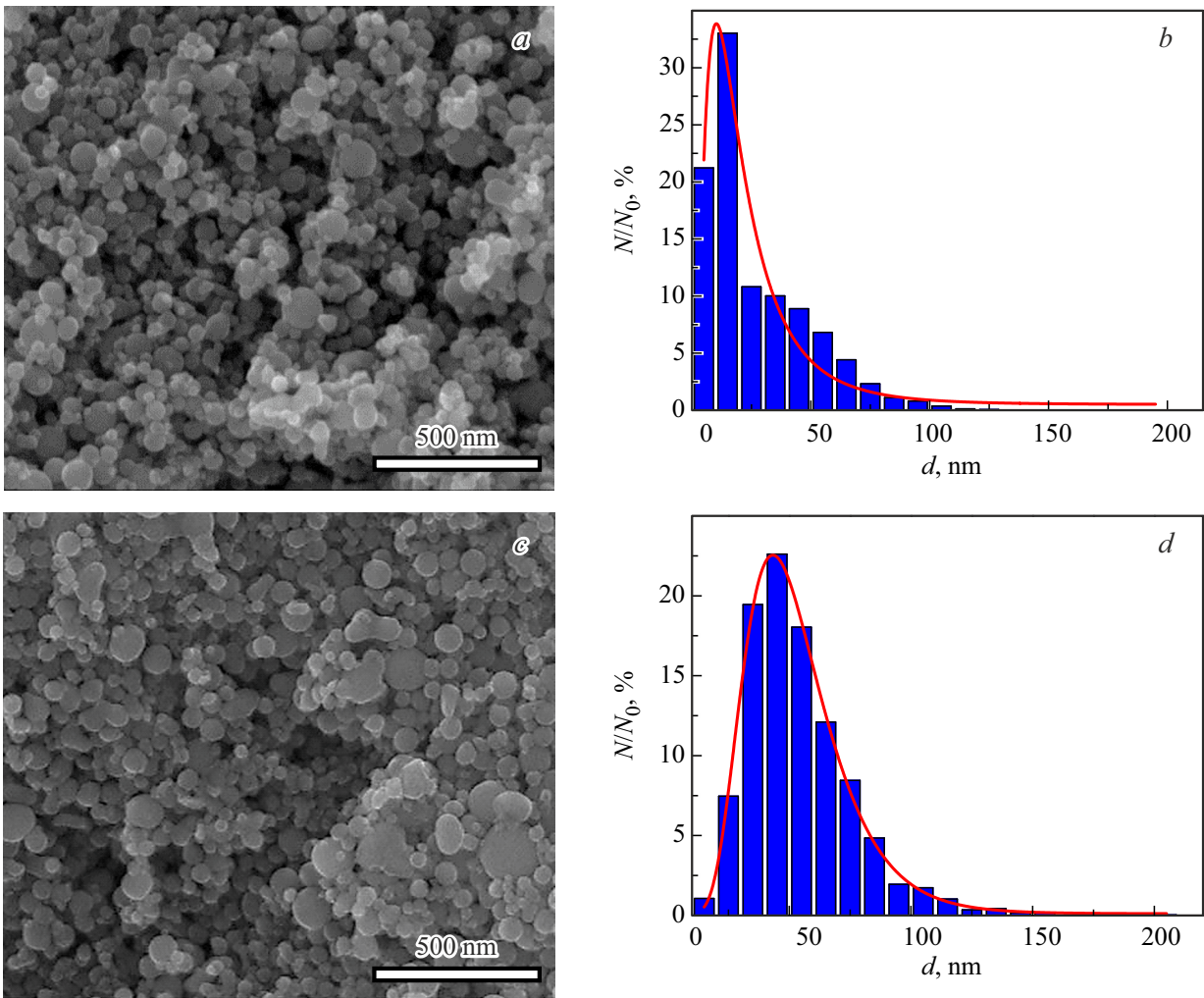
Figure 2. General view (SEM) of the MNP of the batches studied and their corresponding size distributions: a, b — P1; c, d — P2; e, f — P3; g, h — P4. The particle number in the sample (N_0) was P1 — 2522, P2 — 2827, P3 — 2433 and P4 — 2319.

analyzed at a single SEM magnification greater than the magnification used for the qualitative evaluation. Figure 2 shows the SEM photos for all batches and their corresponding size distributions for calculating the average number mean diameter of the MNP batch. The quantitative particle size distributions of all types of particles are well approximated by a lognormal law (fitted with the non-linear LogNormal function). The fitting curve approximated the data well, as evidenced by a coefficient close to one. The dn values of each batch are shown in Table 2.

The smallest average diameter of FeNi magnetic particles is observed for the P1 series. The diagrams show that most of the magnetic particles are in the range of average diameter up to $14-200$ nm. This must take into account the fact that the SEM method underestimates the contributions corresponding to both very large and very small particles. The data obtained are in qualitative agreement with the data on the specific surface area of MNP.

According to the X-ray diffraction analysis (Figure 3), two phases were detected: face-centered cubic γ-phase (spatial

group, S.G: Fm-3m) and body-centered cubic α-phase (S.G: Im-3m). Their percentages differ slightly between samples from different batches (Table 2). The size of the

Table 2. Structural characteristics of different batches of FeNi nanoparticles

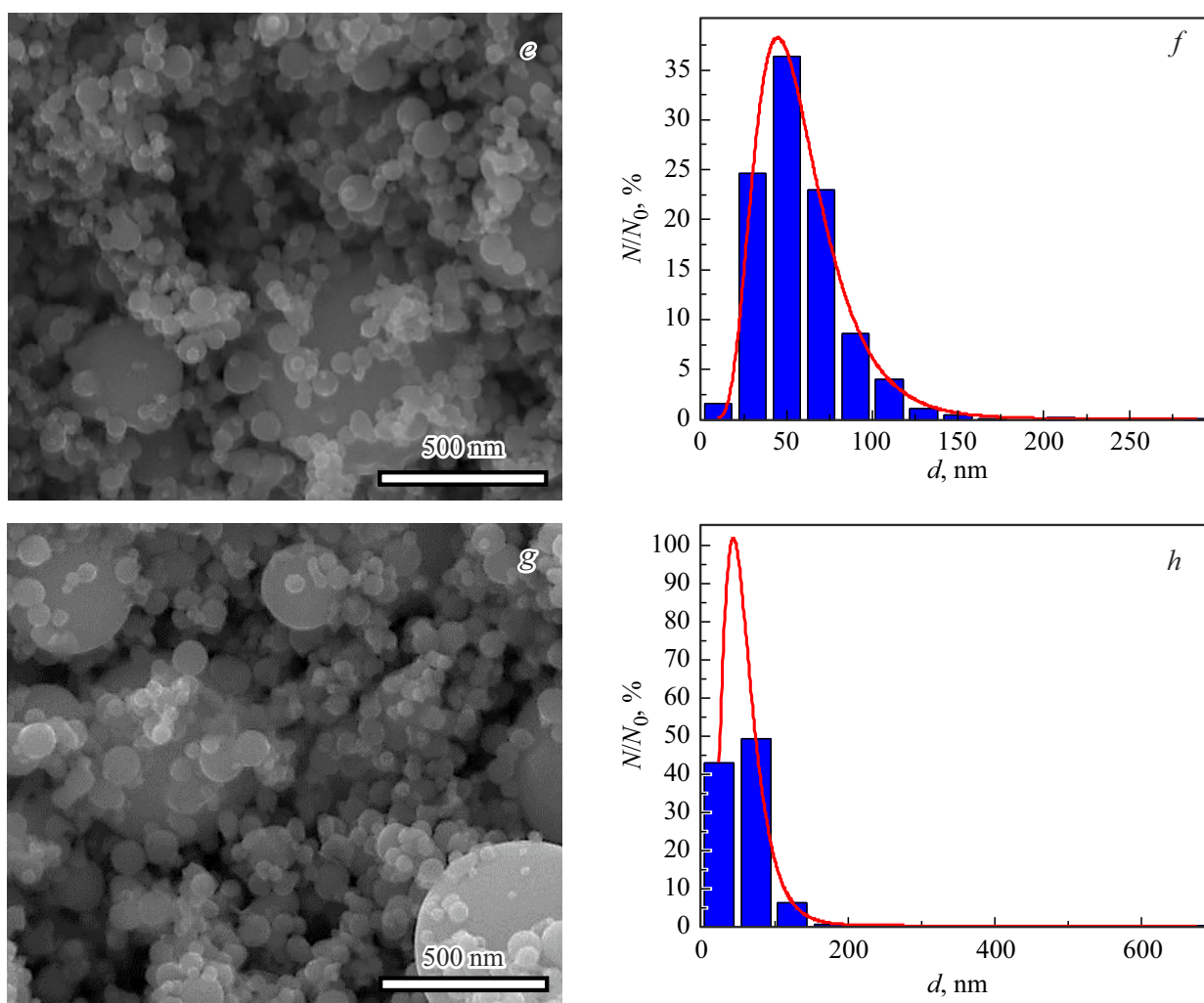| Sample	d_n, nm	Phase	2θ, deg	Phase share,%	d_{cr}, nm
P1	18	γ	43.699	89.3	50
		α	44.836	10.7	50
P2	50	γ	43.693	88.9	55
		α	44.833	11.1	55
P3	53	γ	43.666	92.1	140
		α	44.807	7.9	70
P4	54	γ	43.704	95.5	190
		α	44.829	4.5	80

Figure 2 (*cont.*).

coherent scattering areas for each phase in all (d_{cr}) batches is determined by the Scherrer method. The position of each maximum used for the calculation is also given in Table 2.

Although the average particle size of each batch derived from XRD data is slightly higher than that derived from microscopy data, all of the batch certification methods used lead to the same conclusion: reducing the degree of superheating during MNP production leads to a broadening of the batch size distribution and a shift of the distribution maximum to a larger size range.

Figure 4, a shows the temperature dependence of magnetization (M) for samples P1 and P4 as an example. Note, the gentleness of the initial slope of the curves as the temperature decreases from the Curie temperature (T_C).

This is an indirect confirmation of the wide variation in particle size detected by structural methods, which in turn leads to a wide range of values T_C corresponding to particles of different diameters. For sample P4, the bend in the dependence $M(T)$ confirms the presence of both
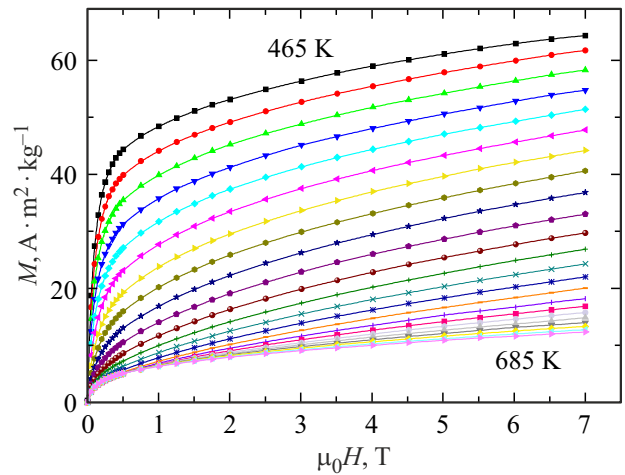
a fraction of relatively large particles and the presence of quite small particles: Figure 4, a clearly shows the presence of two inflection points, which can be interpreted as contributions from particles of different average size. For all samples, the TC value was determined from the minimum of the temperature dependence of the derivative dM/dT. Figure 4, b shows this dependence for samples P1 and P4 as an example. The TC values of all samples were in the range 500 ± 30 K.

Given the defined values T_C, a temperature range of 465 to 685 K was selected in which a set of magnetization curves was measured in 10 K temperature steps. Figure 5 shows the corresponding curves for sample P1. At $T < T_C$, the magnetization shows an intense increase at low fields and then a tendency to saturation at high fields, exhibiting behavior typical of ferromagnetics. As the temperature increases in the interval $T > T_C$, the shape of the curves $M(T)$ tends to linear, which is typical of paramagnetics. This pattern was observed for all the samples tested.
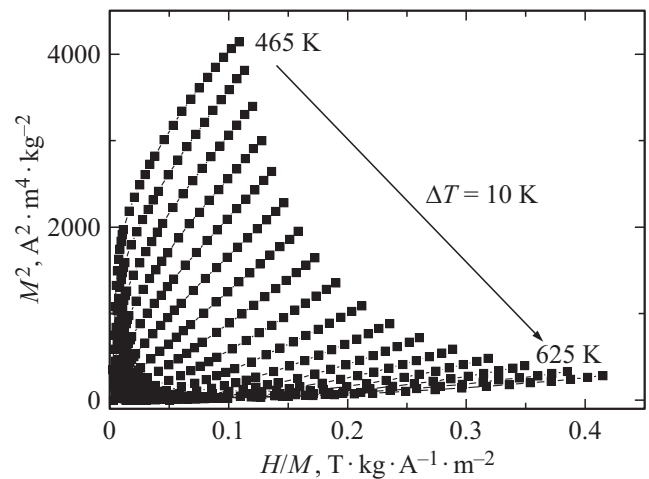
Figure 6 shows the $M(T)$ dependencies for sample P1, reconstructed in Belov's−Arrott coordinates: M^2 from H/M. The curves slope remains positive at all temperatures,
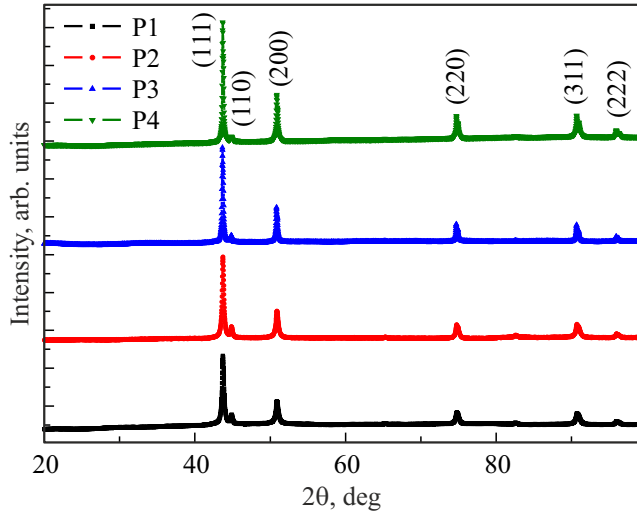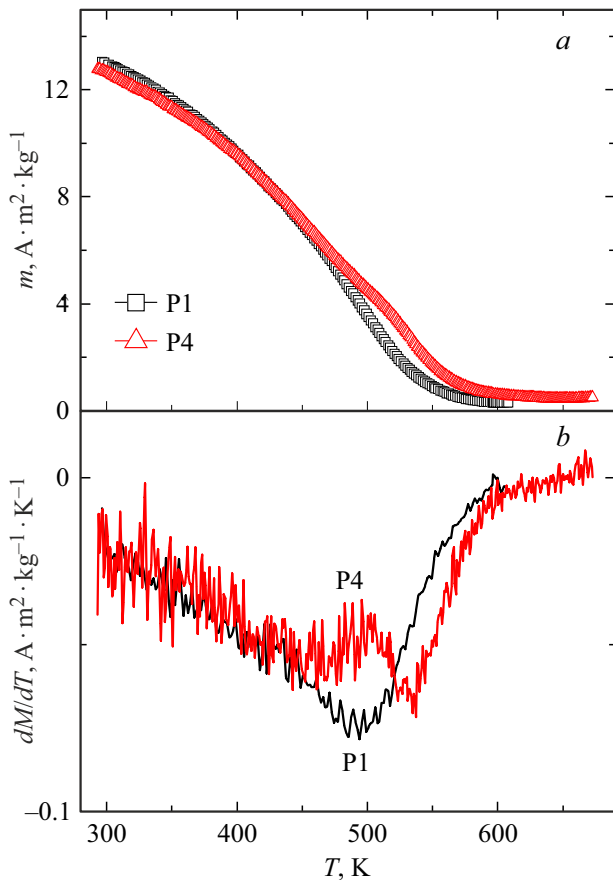

Figure 3. X-ray diffraction patterns of different batches of FeNi EWE-nanoparticles. Miller's indices are shown in brackets.

Figure 4. *a*) Temperature dependencies of magnetization for samples P1 and P4, measured in external magnetic field 0.01 T; *b*) corresponding temperature dependencies of the derivative dM/dT.

Figure 5. Magnetic isotherms for sample P1.

**Figure 6.** Belov-Arrott curves for sample P1.

indicating the presence of a second kind of phase transition in this sample ferromagnetic − paramagnetic near T_C [16]. By extrapolating the Belov − Arrott curves, the Curie temperature for this sample was determined ($T_C \approx 530\,K$); this value is close to that determined from the minimum of the temperature derivative dM/dT. A similar procedure was carried out for all samples; the values T_C determined by this method also fell within the interval $500 \pm 30\,K$.

Based on the magnetization curves, the temperature dependences of the change in the magnetic part of the entropy $\Delta SM(T, H)$ of the studied samples were determined using the known expression [17]:
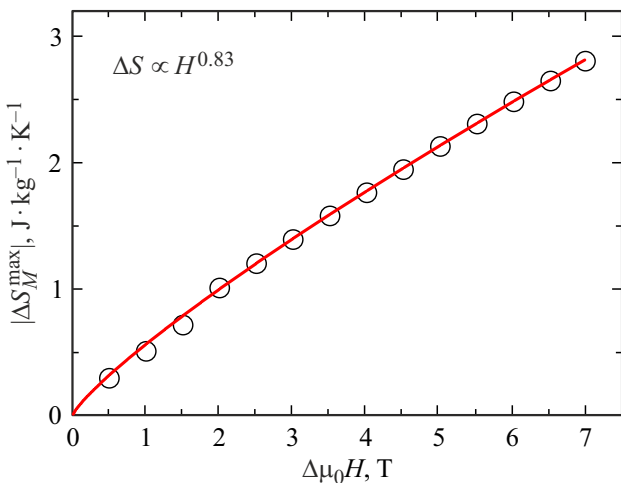
$$\Delta S_M = \int\limits_0^H \left(\frac{\partial M}{\partial T} \right)_H dH, \qquad (3)$$

where M — magnetization, H — magnetic field, T — temperature.

The dependencies $\Delta S_M(T)$ at $\Delta\mu_0 H = 7\,T$ are shown in Figure 7. The maximum values for all samples were
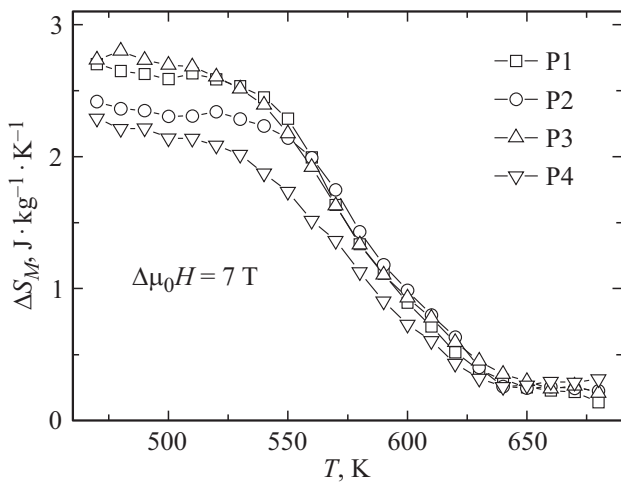
Figure 7. Temperature dependencies of the change in the magnetic part of the entropy for all samples.

Figure 8. Temperature dependencies of the change in the magnetic part of the entropy for all samples.

close and did not differ by more than 15%. The lowest ΔS_M values were observed for sample P4, which has the widest particle size distribution. Perhaps the relatively high proportion of very fine particles is the reason for the reduced ΔS_M for this sample. Note also, that the ΔS_M values obtained for the studied FeNi nanoparticles are about an order of magnitude smaller than those for Gd [3]. On the other hand, with $T < 520\,\mathrm{K}$ ΔS_M remains practically constant when the temperature changes. This can be an advantage for the working material for magnetic cooling according to the so-called Ericsson cycle, where the working material must have a constant high ΔS_M over the entire operating temperature range [18].

As it follows from (3), the MCE magnitude increases with the growth of applied external magnetic field. Another way of improving the efficiency of the magnetic refrigerator — increasing the response to the magnetic field of the material—„of the refrigerant". As shown earlier, this can be achieved by creating multiphase systems [12]. It is known that for magnetocaloric materials characterized by a second order phase transition, the dependence of the magnetic entropy change on the field can be described by a power law: $\Delta S_M \propto H^n$ [19]. Three temperature intervals can be distinguished for single-phase material, which are characterized by their index n in (3.12): at $T \gg T_C$ $n = 2$, at $T \ll T_C$ $n = 1$ and near T_C for the medium field area (tens of kOe) $n = 2/3$ [19]. Figure 8 shows the experimental field dependence of the ΔS_M peak value for sample P1, which can be well described by the power law at $n = 0.83$. The values n for the remaining samples fall within the range of 0.79 to 0.83, which is within the measurement error of the n for bulk Gd [7]. Note also, that the value $\Delta S_M = 0.3\,\mathrm{J/kgK}$ at $\Delta\mu_0 H = 0.5\,\mathrm{T}$ exceeds the analogous parameter for high-entropy FeCoNiCu alloy powders alloyed with Pt [20].

Note again, that we may be talking about multistage cooling (for each temperature step/temperature interval, the working material can be selected separately). In addition, the issue under consideration is interesting in terms of finding additional methods for attestation of large batches of nanoparticles with a wide size distribution.

Assessing the prospects for further research on large batches of EWE nano-powders for magnetocaloric applications, the existing possibilities of improving the MCE properties of these materials through additional treatments should be noted. One of the directions could be the use of mechanic chemistry as a way of alloying the transition metal low-purity alloys with small amounts of Pt or Gd and controlled search for optimal dispersion parameters of large batches.

4. Conclusion

The combination of production conditions and magnetocaloric properties of the studied large batches of FeNi nano-powders produced by electric wire explosion opens up the prospect of using this material in magnetic cooling devices. In addition, the evaluation of the magnetocaloric effect features may be of interest in terms of finding additional methods for the characterization of large batches of nanoparticles with a wide size distribution.

Conflict of interest

The authors declare that they have no conflict of interest.

References

[1] V.V. Sokolovskiy, O.N. Miroshkina, V.D. Buchelnikov, V.V. Marchenkov. Phys. Met. Metallography **123**, *4*, 315 (2022).

[2] L.M. Moreno-Ramírez, J.S. Blázquez, V. Franco, A. Conde, M. Marsilius, V. Budinsky, G. Herzer. J. Magn. Magn. Mater. **409**, 56 (2016).

[3] A.M. Tishin, Y.I. Spichkin, The Magnetocaloric Effect and its Applications. CRC Press, Boca Raton, FL (2003).

[4] I.S. Tereshina, G.A. Politova, V.A. Chetyrbotskii, E.A. Tereshina-Chitrova, M.A. Paukov, A.V. Andreev. Phys. Solid State **61**, *2*, 90 (2019).

[5] O.V. Koplak, S.N. Kashin, R.B. Morgunov, D.V. Korolev, M.V. Zhidkov, V.P. Piskorsky, R.A. Valeev. Phys. Solid State **64**, *11*, 1736 (2022).

[6] M.K. Sharma, A. Kumar, K. Kumari, S. Park, N. Yadav, S.-H. Huh, B.-H. Koo. Appl. Sci. **12**, *18*, 9098 (2022).

[7] J.S. Blázquez, J.J. Ipus, L.M. Moreno-Ramírez, J.M.Álvarez-Gómez, D. Sánchez-Jiménez, S. Lozano-Pérez, V. Franco, A. Conde. J. Mater. Sci. **52**, *20*, 11834 (2017).

[8] S. Wolf, T.M. Riedemann, J. Barclay, J. Holladay, I.E. Anderson, J. Cui. Powder Technol. **359**, 331 (2020).

[9] A.V. Svalov, A.V. Arkhipov, S.V. Andreev, D.S. Neznakhin, A. Larrañaga, G.V. Kurlyandskaya. Mater. Lett. **284**, *Part 1*, 128921 (2021).

[10] G.V. Kurlyandskaya, S.M. Bhagat, A.P. Safronov, I.V. Beketov, A. Larranaga. AIP Adv. **1**, *4*, 042122 (2011).

[11] G.V. Kurlyandskaya, A.P. Safronov, S.M. Bhagat, S.E. Lofland, I.V. Beketov, L. Marcano Prieto. J. Appl. Phys. **117**, *12*, 123917 (2015).

[12] D. Doblas, L.M. Moreno-Ramírez, V. Franco, A. Conde, A.V. Svalov, G.V. Kurlyandskaya. Mater. Design **114**, 214 (2017).

[13] M.A. Kuznetsov, A.B. Drovosekov, A.A. Fraerman. JETP **132**, *1*, 79 (2021).

[14] G.V. Kurlyandskaya, A.P. Safronov, S.V. Shcherbinin, I.V. Beketov, F.A. Blyakhman, E.B. Makarova, M.A. Korch, A.V. Svalov. Phys. Solid State **63**, *10*, 1447 (2021).

[15] Y.-W. Jun, J.-W. Seo, J. Cheon. Accounts. Chem. Res. **41**, *2*, 79 (2008).

[16] B.K. Banerjee. Phys. Lett. **12**, *1*, 16 (1964).

[17] V.K. Pecharsky, K.A. Gschneidner, Jr. J. Appl. Phys. **86**, *1*, 565 (1999).

[18] A. Smaöli, R. Chahine. J. Appl. Phys. **81**, *2*, 824 (1997).

[19] V. Franco, A. Conde. Int. J. Refrig. **33**, *3*, 465 (2010).

[20] M. Kurniawan, A. Perrin, P. Xu, V. Keylin, M. McHenry. IEEE Magn. Lett. **7**, 6105005 (2016).

Translated by Ego Translating